2010

Performance Characteristics and Mapping for a Variable-Speed Ductless Heat Pump

Howard Cheung
Ray W. Herrick Laboratories, Purdue University, howard.at@gmail.com

James E. Braun
Ray W. Herrick Laboratories, Purdue University, jbraun@purdue.edu

Performance Characteristics and Mapping for a Variable-Speed Ductless Heat Pump

Howard Cheung* and James E. Braun

Ray W. Herrick Laboratories, School of Mechanical Engineering, Purdue University
West Lafayette, Indiana, U.S.A.
E-mail: cheung@purdue.edu

* Corresponding Author

ABSTRACT

The paper presents performance characteristics and an approach for mapping the performance of a variable-speed ductless heat pump system (DHP) operating in heating mode. This type of equipment is gaining popularity and is not currently included within building simulation programs that are typically used for design and LEED (Leadership in Energy and Environmental Design) certification. Steady-state performance maps are needed for these simulation tools. Experiments were conducted on a DHP at various conditions and regression analysis was implemented to generate a model. Comparisons were made with data which were not used to derive the model and good accuracy was demonstrated. The resulting performance map was used to demonstrate trends in performance with operating conditions.

1. INTRODUCTION

Despite the use of ductless heat pump systems (DHP) in Asia for decades, their application in the U.S. market has only emerged in recent years. These types of units typically use variable-speed compressors and fans to provide very good part-load performance, which complicates the modeling/mapping of their performance. Nonetheless, prediction of performance is critical in evaluating buildings in the design phase and supporting LEED (Leadership in Energy and Environmental Design) certification for high performance buildings.

Modeling approaches for steady-state performance of heat pump systems can be categorized into three groups: white-box, gray-box and black-box models. White-box models are constructed entirely using physical laws governing the processes within the vapor compression cycle. Pure white-box models were used in the 1970s (Ellison et al., 1976; Hiller and Glicksman, 1976) but are seldom used now because of the complexity associated with the compressor and expansion device modeling. For the design vapor compression equipment, gray-box models are typically employed that consist of a combination of empirical and physical models. Empirical models are usually used for compressors and expansion valves and white or gray-box models are used for heat exchangers (Browne and Bansal, 2007; Ding, 2007; Shen, 2006). However, these gray box models are not typically used in simulating building performance because of their complexity and computational requirements.

Black-box models are composed entirely of empirical models and therefore do not generally utilize parameters that have physical meaning. However, they can map the performance of a system that has been tested and provide very fast execution speeds compared to gray or white-box models. As a result, black-box models are generally utilized in system simulation programs. General procedures for developing regression models for vapor equipment have been presented (Reddy and Anderson, 2002) and alternative minimization functions have been proposed (Swider, 2003).

The current paper develops a simple empirical model for a ductless heat pump operating in heating mode that was tested within the laboratory. Some of the data were used for the model construction process and additional data were compared with the model prediction for model verification. The resulting model was then used to demonstrate performance trends for the unit.

2. EXPERIMENTAL SET-UP AND PROCEDURE

To obtain data for construction and verification of an empirical model, experiments on a small 1 ton DHP that has a single indoor heat exchanger were performed within the psychrometric chambers at the Herrick Laboratories, Purdue University. Sensors were installed within the refrigerant circuit as shown in Figure 1.

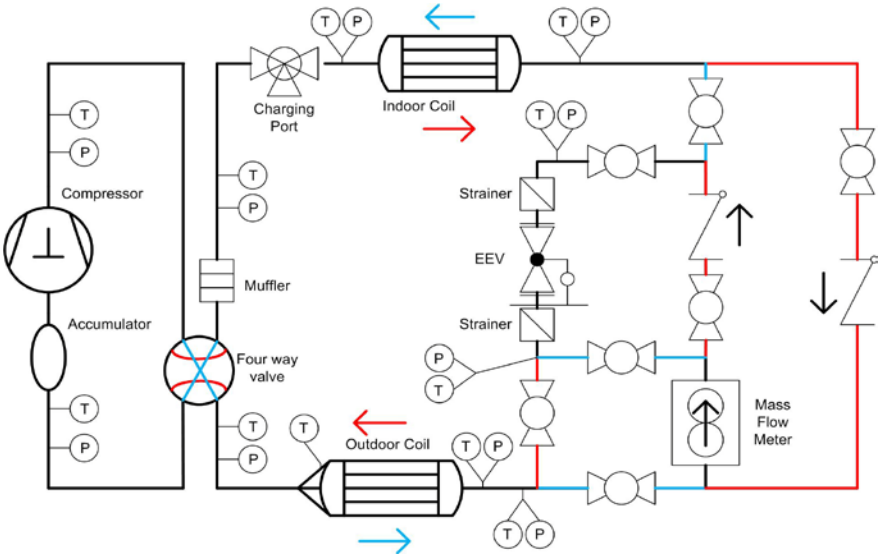

Figure 1 Schematic of refrigerant circuit for experiments

T-type Thermocouples with ±1.0°C error and pressure transducers with ±0.25% on full scale were installed to obtain the refrigerant-side properties in the cycle. A coriolis mass flowmeter was also installed at the outlet of the condenser for refrigerant mass flow rate. Air properties at the inlet and outlet of the indoor unit were measured using arrays of thermocouples and a dew point sampling pump. Airflow across the unit was measured using a nozzle apparatus as described in ASHRAE Standard 41.2. Power meters were also installed to measure power to the indoor and outdoor unit.

The unit was operated in heating mode at steady state with different compressor powers, fan speeds and outdoor air temperatures and at least 10 minutes of steady-state data were obtained at a 10s interval for each scenario. The indoor room was kept at a dry bulb temperature of 21°C (70°F) (dry room) in the heating tests. The test matrix for developing the model is shown in Table 1. The outdoor unit power includes the compressor and outdoor fan power and is shown to indicate the operating speed of the compressor since the speed was not directly measured. The indoor air flow was directly specified, whereas the compressor speed was indirectly manipulated by adjusting the setpoint temperature for the indoor room. A high setpoint temperature (31°C/ 88°F) was specified to achieve the maximum compressor speed whereas the minimum was reached with a setpoint temperature equal to the room temperature (21°C/ 70°F). Intermediate speeds were realized by changing the setpoint temperature from 23 °C to 21°C (74°F to 70°F) when the outdoor unit power was increasing from its minimum.

Table 1 Test matrix

Outdoor Temperature (°C)	Compressor Speed	Air Flow Rate	Outdoor unit power achieved (kW)
18	Minimum	High	0.208
17	Maximum	High	1.758
	Maximum	Medium	1.522
	Intermediate	Medium	0.816
	Minimum	Medium	0.226
	Maximum	Low	1.237
	Intermediate	Low	0.603
	Minimum	Low	0.250
8	Maximum	High	1.891
	Maximum	Low	1.079
	Minimum	Low	0.238
2	Maximum	High	2.124
	Intermediate	Medium	1.177
	Minimum	Low	0.405
-3	Maximum	High	2.161
	Maximum	Medium	1.789
	Intermediate	Medium	1.151
	Maximum	Low	0.915
-8	Maximum	High	2.157
	Maximum	Medium	1.511
	Minimum	Medium	1.048
-9	Maximum	Medium	1.024
-14	Maximum	Low	2.164

3. EMPIRICAL MODELING APPROACH

The modeling was separated into two parts: i) models for capacity and power with the unit operating at maximum compressor and fan speeds and ii) a model for power consumption in terms of relative load and fan speed. This decoupling approach reduced the number of empirical parameters necessary to map the performance. The maximum heating capacity and associated power input were found to be linear functions of the outdoor temperature. A linear regression was carried out on the data with maximum indoor unit airflow and maximum compressor speed to calculate the coefficients of equations (1) and (2).

$$W_{\max} = A_0 + A_1 T_{outdoor} \tag{1}$$

$$Q_{\max} = A_2 + A_3 T_{outdoor} \tag{2}$$

The power consumption relative to the maximum power consumption was represented using a polynomial model in terms of relative indoor fan speed and relative load (part-load ratio). The process started with the polynomial shown in equation (3) and then this equation was simplified using statistical analysis.

$$\frac{W}{W_{\max}} = C_0 + C_1\frac{Q}{Q_{\max}} + C_2\frac{V}{V_{\max}} + C_3\left(\frac{Q}{Q_{\max}}\right)^2 + C_4\left(\frac{V}{V_{\max}}\right)^2 + C_5\left(\frac{Q}{Q_{\max}}\right)\left(\frac{V}{V_{\max}}\right) + C_6\left(\frac{Q}{Q_{\max}}\right)^3 + C_7\left(\frac{V}{V_{\max}}\right)^3 + C_8\left(\frac{Q}{Q_{\max}}\right)^2\left(\frac{V}{V_{\max}}\right) + C_9\left(\frac{Q}{Q_{\max}}\right)\left(\frac{V}{V_{\max}}\right)^2 \tag{3}$$

The verification of data for ill-conditioning was examined by calculating the condition number of the data as shown in equations (4) and (5). Since the entries of equation (3) are inter-related, only the basic components of the entries

(Q/Q_{max} and V/V_{max}) are considered. A condition number larger than 15 implies ill-conditioned data.

$$\text{Condition number} = \sqrt{\frac{\text{Largest Eigenvalue of A}}{\text{Smallest Eigenvalue of A}}} \tag{4}$$

where

$$A = \begin{pmatrix} \frac{Q}{Q_{\max 1}} & \frac{V}{V_{\max 1}} \\ \vdots & \vdots \\ \frac{Q}{Q_{\max N}} & \frac{V}{V_{\max N}} \end{pmatrix}$$

The coefficients were obtained by regression with steady-state data. After calculating the coefficients in the model, the model was simplified by reducing the covariates. This was carried out by backward elimination and Cp statistics (Wu and Hamada, 2000). In Cp statistics, covariates were eliminated from the model with the Cp computed using equation (5).

$$C_p = \frac{RSS}{s^2} - (N - 2p) \tag{5}$$

The model with the smallest difference between Cp and p became the simplified model. However, to save computational effort, only models processed during backward elimination were analyzed in this way.

In backward elimination, models with one less covariate were constructed and a variable called partial F was calculated using equation (6) from each of the smaller models.

$$\text{partial F} = \frac{RSS - RSS_o}{RSS_o} v \tag{6}$$

The one with the smallest partial F replaced the larger model and the process was repeated until all the partial Fs were larger than an F-value that depends on the degree of freedom of smaller models and a critical value according to the F-distribution as shown in Table 2. The critical value marks the standard to eliminate covariates. A higher critical vale implies stricter rules to remove a covariate and in general, a value between 0.1 and 0.2 is recommended. The last model for the replacement was compared with the one generated from the Cp statistics and the more accurate one was selected as the model. The resulting model was then used to predict the performance at data points not used in the regression process.

Table 2 F-value for comparison

First parameter for F-distribution	Second parameter for F-distribution: Degree of freedom of smaller models	Upper critical value	F-value
1	8	0.2	1.91
	7		1.95
	6		2.00
	5		2.07

4. RESULTS AND DISCUSSION

Coefficients of equations (1) and (2) determined through the regression analysis are shown in Table 3. Five data points with high fan speed at different outdoor temperatures with maximum compressor speed and fan speeds were utilized for the regression. These data and the model prediction are plotted in Figure 2. The heating capacity increases linearly with outdoor air temperature and varies by about 25% over the units range of operation. The maximum power consumption decreases linearly with increasing outdoor temperature due to more efficient operation.

Table 3 Coefficients and r^2 for the experimental unit in equations (1) and (2) with output in kW and input in °C

Equation (1)		Equation (2)	
A_0	2.07540	A_2	5.56010
A_1	-0.01784	A_3	0.06123
r^2 for (1)	89.75%	r^2 for (2)	95.10%

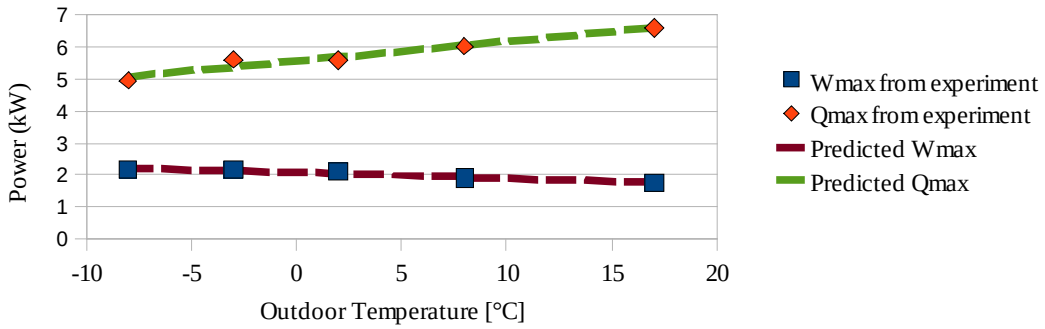

Figure 2 Comparison of model prediction and data for Equations (1) and (2)

The low r^2 is a result of the small sampling size used to determine the coefficients of the regression model. The maximum relative errors for the models of equations (1) and (2) are 3.97% and 4.01%, respectively, and the mean standard deviations for the error are 1.01% and 1.78%.

The regression procedure utilized 19 data points with 5 additional data points used for model testing. Based on the data, the applicable range of the model in terms of relative loads for different fan speeds is tabulated in Table 4.

Table 4 Applicable range of Q/Qmax

Fan speed	Range
High	1.00 – 0.81
Medium	0.89 – 0.30
Low	0.70 – 0.28

The data for regression were analyzed and the condition number was found to be 8.831, meaning that the data are not ill-conditioned for the regression model.

The simplified polynomial regression model determined from the aforementioned statistical methods is given in equation (7).

$$\frac{W}{W_{max}} = C_0 + C_1\frac{Q}{Q_{max}} + C_2\left(\frac{Q}{Q_{max}}\right)^2 + C_3\left(\frac{Q}{Q_{max}}\right)\left(\frac{V}{V_{max}}\right) + C_4\left(\frac{Q}{Q_{max}}\right)^3 + C_5\left(\frac{V}{V_{max}}\right)^3 + C_6\left(\frac{Q}{Q_{max}}\right)\left(\frac{V}{V_{max}}\right)^2 \quad (7)$$

The coefficients of equation (8) determined from regression are listed in Table 5. The r^2 for the model is 99.85%, revealing good regression results.

Table 5 Coefficients for equation (7)

Coefficients	Values	Coefficients	Values
C_0	0.0914	C_4	-0.8678
C_1	0.8033	C_5	0.1902
C_2	2.5976	C_6	1.4833
C_3	-3.2925		

The agreement between model predictions and measurements of outdoor unit power consumption is illustrated in Figure 3. The maximum absolute error in power consumption is about 88W for data used for model construction and 75W for other data. The mean standard deviation for the error using all the data is 24W. On average, the errors are relatively small compared to the maximum power consumption of around 2kW and the model works well in predicting power.

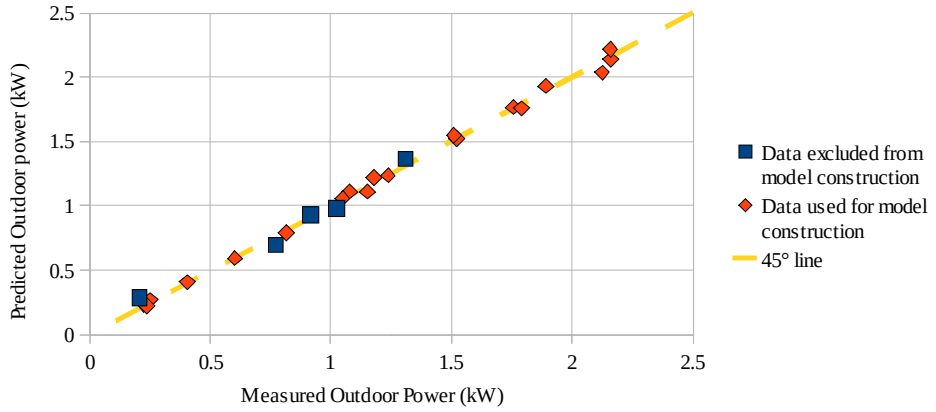

Figure 3 Comparison of outdoor power consumption between model predictions and measurements

To illustrate the steady-state performance of the unit in heating mode, coefficient of performance (COP) at different indoor fan speeds and Q/Q_{max} are shown as a function of outdoor air temperature in Figures 4 to 6. The steady-state performance is excellent even at low ambient temperatures that are well below the freezing point of water. At high fan speed, the best COP is achieved at a part-load ratio (Q/Q_{max}) of about 50%. In general, lower loads lead to small temperature differences between refrigerant and air flow streams for both heat exchangers, which tends to improve COP. However, at low loads compressor and motor efficiency are reduced. These tradeoffs can lead to an optimum part-load ratio that depends on the fan speed. For the medium and low speed fan settings, the highest COPs in Figures 4 and 5 occur at a part-load ration of 25%. It is also interesting to note that there is an optimal fan speed that depends on part-load ratio and outdoor temperature. The optimum moves towards higher fan speeds at lower outdoor temperatures and higher loads. For example, the maximum COP at high outdoor temperature and low part-load ratios occurs at the medium indoor fan speed.

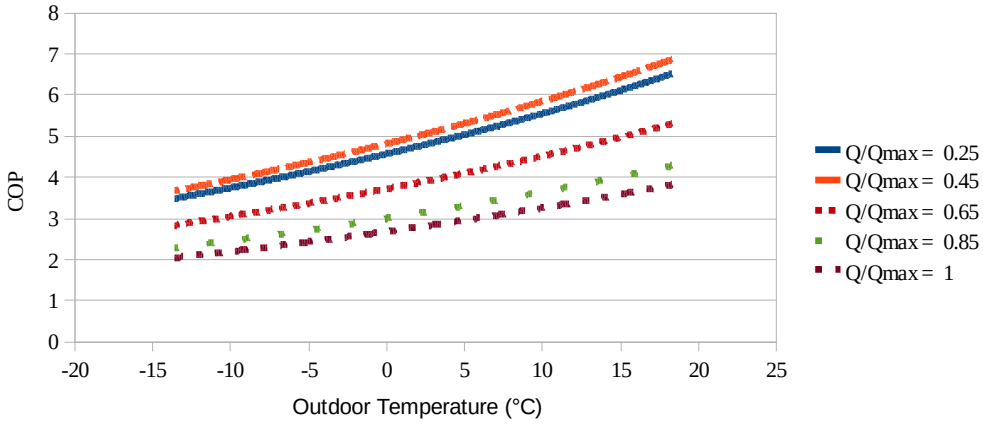

Figure 4 COP as a function of outdoor temperature at high airflow in heating mode

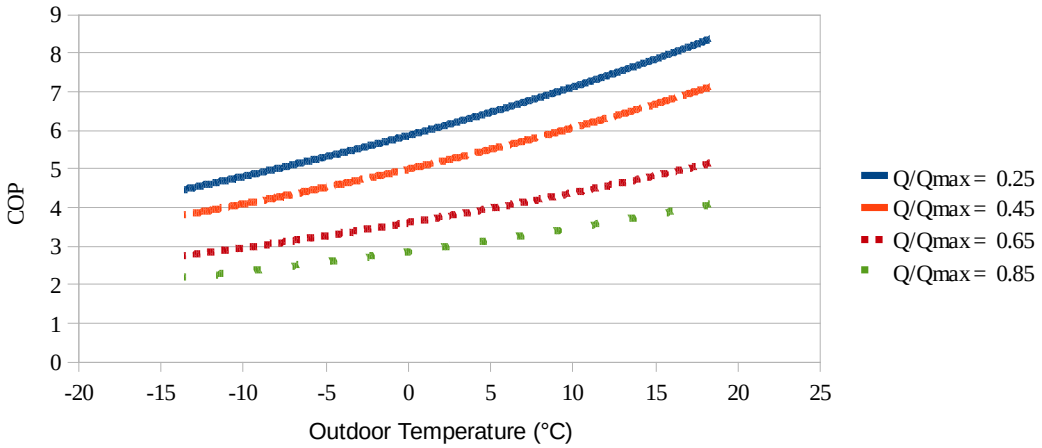

Figure 5 COP as a function of outdoor temperature at medium airflow in heating mode

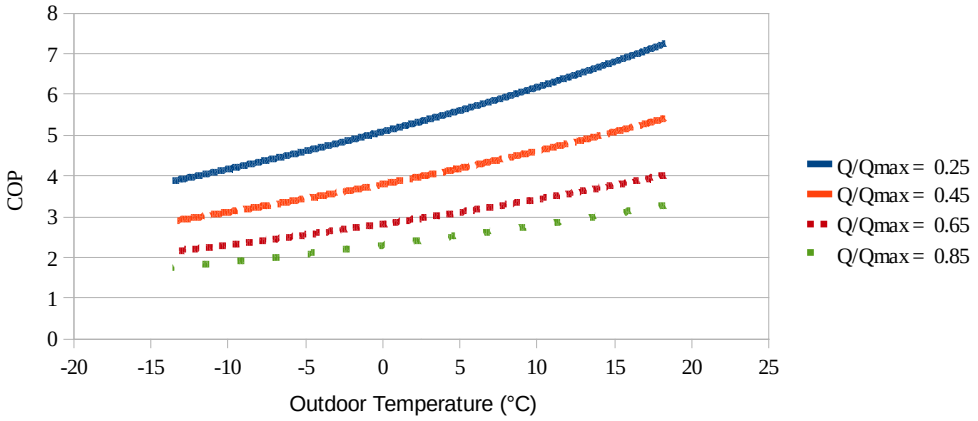

Figure 6 COP as a function of outdoor temperature at low airflow in heating mode

6. CONCLUSIONS

This paper presented an empirical model for a variable-frequency driven ductless heat pump system operating in heating mode. Regression analysis was used to construct the model and experimental data were used for the development and verification of the model. The mapping of the model was also explored and analyzed for the effect of airflow and heating load on system COP. It was shown that there is an optimal load for maximum COP that depends on the indoor fan speed. It is expected that the optimal loading for maximum COP results from a tradeoff between reduced refrigerant-to-air temperature differences in the heat exchangers and reduced compressor and motor efficiencies that occur with decreased loading. For a given load and outdoor temperature, there is also an optimum indoor speed. For the most of the operating range, the optimal fan speed is the high speed for this particular unit. However, the optimal speed is medium speed at higher outdoor temperatures and lower loads. The model developed in this study could be easily implemented within a building simulation program in order to evaluate the benefits of this technology within the U.S. market as compared with more conventional equipment that is typically utilized.

NOMENCLATURE

A_i	regression coefficients in the relation of the maximum power to the outdoor temperature	
C_i	regression coefficients in the empirical model	
N	number of observations	
υ	degree of freedom of the smaller model	
p	number of regression coefficients	
Q	heat output	(kW)

RSS residual sum of squares of the model
RSS_o residual sum of squares of the larger model in the backward elimination process
r^2 coefficient of determination
s^2 mean square error of the model shown in (3)
T temperature (°C)
V airflow across indoor unit (m^3/s)
W power input to the unit (kW)

Subscripts

max maximum
outdoor outdoor room condition

REFERENCES

Air Conditioning, Heating, and Refrigeration Institute., 2008, *2008 Standard for Performance Rating of Unitary Air-Conditioning & Air-Source Heat Pump Equipment*, AHRI Standard 210/240.

American Society of Heating, Refrigerating and Air-Conditioning Engineers, Inc., 1987, *Standard Methods for Laboratory Airflow Measurement*, ANSI/ASHRAE 41.2-1987 (RA 92).

Browne, M. W., Bansal, P. K. , 1998, Challenges in Modeling Vapor-Compression Liquid Chillers. ASHRAE Transactions. 104: 474 – 486

Cheung, H., , Kim., W. And Braun, J. E.., 2010, Performance Testing of Ductless Heat Pumps Progress Report for February, 2010, Internal Report, Herrick Laboratories, Purdue University.

Ding, G. L., 2007, Recent Developments in simulation techniques for vapour-compression refrigeration systems, *International Journal of Refrigeration*, 30, 1119 – 1133.

Ellison, R. D., 1979, Heat Pump Modeling: A Progress Report, *Proceedings of the 4th Annual Heat Pump Technology Conference*. Stillwater, Oklahoma.

Hiller, C. C., Glicksman, L. R., 1976, *Improving heat pump performance via compressor capacity control : analysis and test*.

Reddy, T. A., Anderson, K. K., 2002, An Evaluation of Classical Steady-State Off-line Linear Parameter Estimation Methods Applied to Chiller Performance Data, *HVAC&R Research*, 8, 1: 101 – 124.

Shen, B., 2006, *Improvement and Validation of Unitary Air Conditioner and Heat Pump Simulation Models at off-Design Conditions*, Ph.D. thesis, Herrick labs, Purdue University.

Swider, D. J. , 2003, A Comparison of Empirically Based Steady-State Models for Vapor-Compression Liquid Chillers, *Applied Thermal Engineering*, 23: 539 – 556.

ACKNOWLEDGEMENT

We would like to acknowledge Woohyun Kim and David Yuill for their help in gathering data for the ductless heat pump system.